Comput Geosci (2016) 20:1287–1300
DOI 10.1007/s10596-016-9590-3

ORIGINAL PAPER

A stochastic inversion workflow for monitoring the distribution of CO_2 injected into deep saline aquifers

Lorenzo Perozzi[1] · Erwan Gloaguen[1] · Bernard Giroux[1] · Klaus Holliger[2]

Received: 18 April 2016 / Accepted: 8 September 2016 / Published online: 4 October 2016

Abstract We present a two-step stochastic inversion approach for monitoring the distribution of CO_2 injected into deep saline aquifers for the typical scenario of one single injection well and a database comprising a common suite of well logs as well as time-lapse vertical seismic profiling (VSP) data. In the first step, we compute several sets of stochastic models of the elastic properties using conventional sequential Gaussian co-simulations (SGCS) representing the considered reservoir before CO_2 injection. All realizations within a set of models are then iteratively combined using a modified gradual deformation algorithm aiming at reducing the mismatch between the observed and simulated VSP data. In the second step, these optimal static models then serve as input for a history matching approach using the same modified gradual deformation algorithm for minimizing the mismatch between the observed and simulated VSP data following the injection of CO_2. At each gradual deformation step, the injection and migration of CO_2 is simulated and the corresponding seismic traces are computed and compared with the observed ones. The proposed stochastic inversion approach has been tested for a realistic, and arguably particularly challenging, synthetic case study mimicking the geological environment of a potential CO_2 injection site in the Cambrian-Ordivician sedimentary sequence of the St. Lawrence platform in Southern Québec. The results demonstrate that the proposed two-step reservoir characterization approach is capable of adequately resolving and monitoring the distribution of the injected CO_2. This finds its expression in optimized models of *P*- and *S*-wave velocities, density, and porosity, which, compared to conventional stochastic reservoir models, exhibit a significantly improved structural similarity with regard to the corresponding reference models. The proposed approach is therefore expected to allow for an optimal injection forecast by using a quantitative assimilation of all available data from the appraisal stage of a CO_2 injection site.

Keywords CO_2 sequestration · Stochastic inversion · Gradual deformation · VSP

1 Introduction

One of the major challenges associated with the large-scale deployment of carbon capture and storage (CCS) operations is the evaluation of the reservoir properties and the forecasting of the spatial distribution of the injected CO_2 plume over time. Adequate knowledge of the rock physical properties at the storage site is crucial for determining the optimal rate of CO_2 injection, which in turn influences the rate of capture as well as the associated monitoring operations. Indeed, most jurisdictions involved in CCS projects require more or less elaborate monitoring, verification, and accounting (MVA) programs (e.g., EU [19]). In this context, arguably the most important and most challenging task is the temporal monitoring of the spatial distribution of the injected CO_2. To date, the characteristics of CO_2 plumes estimated through such monitoring efforts are often inconsistent with corresponding multi-phase fluid flow simulations (e.g., Ramirez

✉ Lorenzo Perozzi
lorenzo.perozzi@gmail.com

[1] Institut National de la Recherche Scientifique, Centre Eau Terre Environnement, 490, rue de la Couronne, Québec, QC, G1K 9A9, Canada

[2] Applied and Environmental Geophysics Group, Institute of Earth Sciences, University of Lausanne, 1015 Lausanne, Switzerland

et al. [55]). This is mainly due to the lack or sparseness of direct measurements of the reservoir properties and the low spatial resolution and coverage of geophysical surveys as well as the uncertainties associated with the modeling and inversion of such data (e.g., Doyen [17]). To evaluate the performance of a reservoir in terms of its capacity for CO_2 storage, corresponding models also need to be constrained by data measured during and/or after the injection operations and must match the observed dynamic behavior of the reservoir within a given tolerance interval.

The process of optimizing a reservoir model to fit dynamic data, such as pressure and water-cut, is commonly known as history matching (e.g., Le Ravalec [37]). History matching is extensively used in the oil and gas industry and is generally based on data from at least one injection and one production well (e.g., Roggero and Hu [57]). History matching requires adequate knowledge of the static reservoir properties in general and of the porosity and permeability in particular. Due to the complexity of the spatial distribution of the rock physical properties and the scarcity of direct observations at the well sites, probabilistic approaches tend to be most suitable (e.g., Doyen [17]). In most CCS projects, only one single injection well is available and hence only indirect constraints, generally based on vertical seismic profiling (VSP) and/or seismic reflection surveys, can be used to improve the characterization of the dynamic behavior of the CO_2 plume (e.g., Lumley et al. [41]).

While it is widely accepted that seismic measurements are well-suited for reservoir characterization and monitoring due to their spatially extensive coverage and sensitivity to density and porosity (e.g., Doyen [17]), the estimation of rock physical properties from such data is a complex and ill-conditioned nonlinear inverse problem. This is notably due to the limited bandwidth and aperture of typical surfaced-based seismic measurements as well as to the presence of noise in conjunction with the inherent simplifications associated with the underlying forward modeling algorithms (e.g., Tarantola [58]).

Seismic inverse problems for reservoir characterization may be addressed following either deterministic or probabilistic approaches and are generally divided into two main categories: (1) multi-step inversion methods and (2) stochastic inversion methods (e.g., Grana et al. [26]). In multi-step inversion methods, the problem of estimating reservoir properties from seismic data is split into two or more sub-problems. Generally, elastic properties are first derived from seismic data, which are then used to infer reservoir properties through stochastic techniques, such as Bayesian classification (e.g., Avseth et al. [1]; Mukerji et al. [48]; Buland and Omre [7]). Iterative stochastic inversion methodologies solve the seismic inverse problem using deterministic or stochastic optimization techniques. First, a set of equivalent models are simulated using a stochastic algorithm based on prior information, usually from well log data as well as from assumptions and/or constraints regarding spatial continuity (e.g., Bosch et al. [5]). Then, rock physics transforms are applied to estimate the elastic properties. Finally, synthetic seismic data are iteratively computed and compared to the corresponding observed data. Several optimization methods exist to infer the elastic properties from seismic measurements. A number of studies have used the Markov chain Monte Carlo approach for the stochastic exploration of the model space (e.g., Eidsvik et al. [18]; Larsen et al. [36]; Gunning and Glinsky [28]; Rimstad and Omre [56]; Ulvmoen and Omre [60]; Hansen et al. [30]). González et al. [25] performed a trace-by-trace deterministic optimization, while Bosch et al. [5] proposed an iterative optimization based on Newton's method. Grana et al. [26] illustrated the efficiency of the probability perturbation method [8] to estimate fine-scale reservoir models. A multi-dimensional scaling technique was successfully applied by Azevedo et al. [2] to assess how the parameter model space is explored by a global elastic inversion algorithm.

In this paper, we propose a stochastic inversion workflow using a gradual-deformation-based optimization technique [57] to assimilate a conceptual geological model, geophysical well logs, VSP data, and flow simulations for monitoring the injection and propagation of CO_2 in a deep saline aquifer. In the following, we first outline the proposed inversion approach and then apply it to a realistic synthetic case study based on data from a potential CCS site in the St. Lawrence Lowlands, Québec, Canada.

2 Methodology

The stochastic inversion procedure we propose is schematically illustrated in Fig. 1. The global workflow comprises two distinct steps. In the first step, which corresponds to the static optimization, that is, before the injection of CO_2, many sets of initial realizations of the reservoir model are simulated from available well log data as well as from geological and geophysical a priori information using a geostatistical co-simulation algorithm. It is important to note that the geological a priori information could consist of multiple scenarios. An optimization procedure is then applied to each of these sets of initial models realizations in order to obtain static models of the reservoir properties that minimize the mismatch between the observed and simulated raw seismic traces before the injection of CO_2. In the second step, which corresponds to the dynamic optimization, the resulting optimized static reservoir models are combined through an iterative history matching procedure where, at each iteration, we simulate the injection and transport of CO_2, compute the rock physical properties of

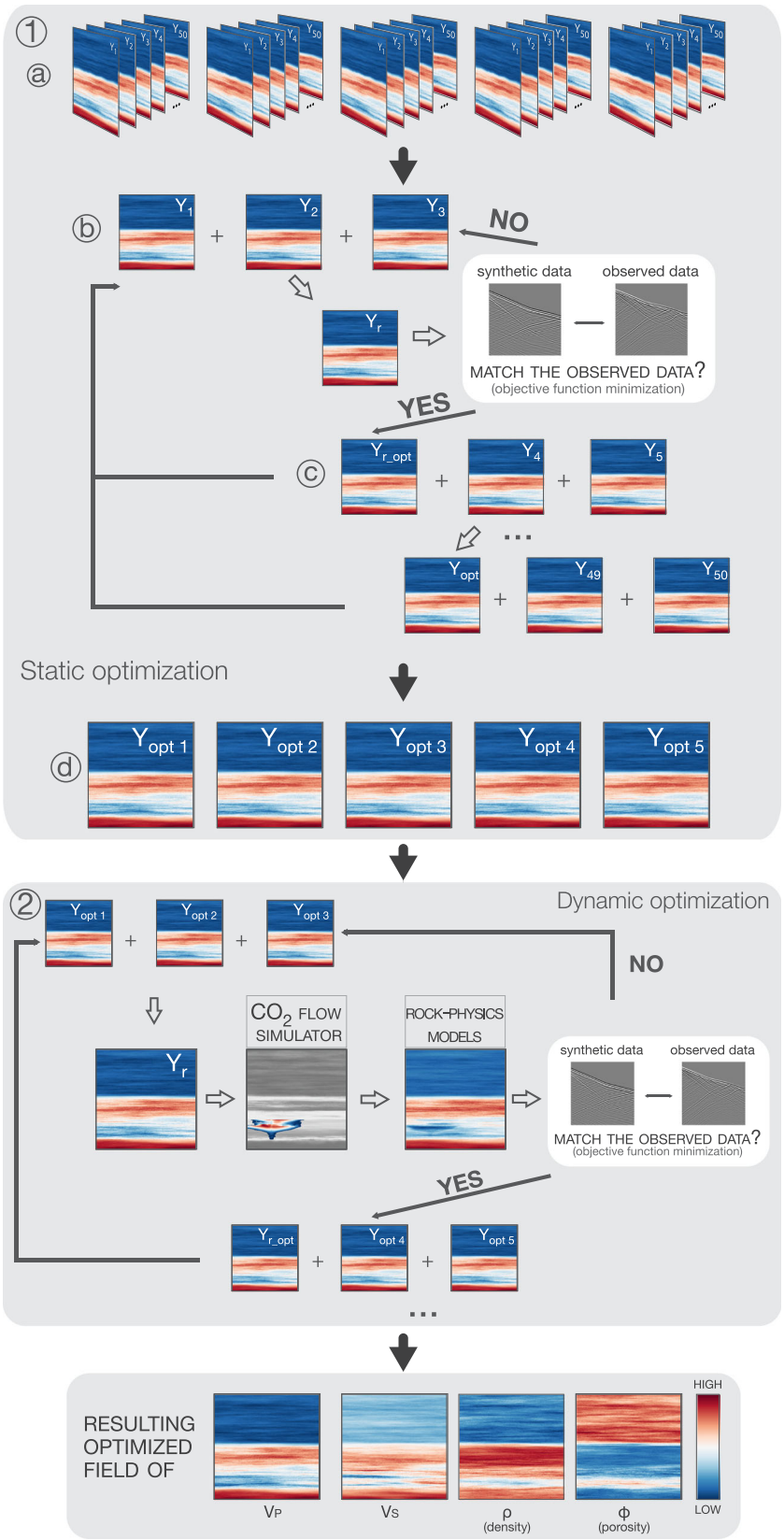

Fig. 1 Schematic illustration of the workflow of the proposed two-step stochastic inversion methodology: *1a* multiple sets of initial reservoir models are generated using sequential Gaussian co-simulation (SGCS); *1b* all sets of previously generated stochastic realizations are iteratively combined using a gradual conditioning (GC) approach; *1c* this procedure is repeated until all initial realizations have been combined together; *1d* we thus ultimately obtain a reservoir model consisting of V_p, V_s, ρ, and ϕ fields that minimize the mismatch between the synthetic and the observed seismic data. *2* We used the same GC approach for the dynamic optimization in order to obtain the spatial distributions of V_p, V_s, ρ, and ϕ that best honor the static and dynamic data

the corresponding reservoir model, and run a seismic forward model to evaluate the mismatch between simulated and observed seismic traces. In the following, we provide a detailed description of the different parts of the proposed stochastic inversion approach.

2.1 Initial reservoir models

The spatial distributions of the P- and S-wave velocities V_p and V_s, the porosity ϕ, and the density ρ for multiple sets of initial reservoir models are generated using sequential Gaussian co-simulation (SGCS) (e.g., Deutsch and Journel [16]; Doyen [17]). Starting from corresponding static information available from well logs and the conceptual geological model, which, in the considered case, consists of a succession of sub-horizontal sedimentary units, the algorithm visits each node of the gridded model space along a random path co-simulating a value for each variable. These co-simulations are conditioned to the measured well log data such that, in addition to being consistent with the second-order statistical characteristics of the observed data, they reproduce the corresponding observations at the well locations. For each set, multiple simulations are generated by using different random seeds in order to obtain independent sets of realizations. This is illustrated in step 1a of Fig. 1.

2.2 Static optimization

All sets of previously generated stochastic realizations are then iteratively combined using a modified gradual deformation (GD) approach in order to minimize the mismatch between the observed seismic data and the corresponding simulations prior to the injection of CO_2 [32]. The GD method was first developed for history matching purposes [57] and involves the linear combination of Gaussian random fields with weights that are adjusted to minimize the mismatch between simulated and observed data while preserving the second-order statistical characteristics of the original models (e.g., Roggero and Hu [57]; Hu [32, 33]; Hu et al. [34]; Le Ravalec et al. [39]; Le Ravalec and Mouche [38]). The key idea behind GD is that the sum of two Gaussian random fields Y_1 and Y_2 is also a Gaussian random field

$$Y(r) = Y_1 \cos(r) + Y_2 \sin(r), \tag{1}$$

where $r \in [-\pi, \pi]$ is the deformation parameter. It can be shown that $Y(r)$ has the same mean and covariance as Y_1 and Y_2 regardless of the value of r, because Y_1 and Y_2 are independent and the sum of the squared combination of the cos- and sin-terms is one. In its classical form, GD involves the combination of independent stochastic realizations only, which implies that the resulting realizations are unconditional. To combine conditional stochastic realizations, a variant of GD, known as gradual conditioning (GC), was developed by Ying and Gomez-Hernandez [63] and Hu [33]. Hu [33] proposes the following weights satisfying these constraints

$$\begin{cases} \alpha_1 = \dfrac{1}{3} + \dfrac{2}{3}\cos(r), \\ \alpha_2 = \dfrac{1}{3} + \dfrac{2}{3}\sin\left(-\dfrac{\pi}{6} + r\right), \\ \alpha_3 = \dfrac{1}{3} + \dfrac{2}{3}\sin\left(-\dfrac{\pi}{6} - r\right). \end{cases} \tag{2}$$

such that

$$Y = \alpha_1 Y_1 + \alpha_2 Y_2 + \alpha_3 Y_3, \tag{3}$$

provides a framework for parameterizing directly conditional stochastic realizations as illustrated by step 1b in Fig. 1. The thus resulting stochastic realization Y is then conditioned to the observed data and consistent with the second-order statistics of the underlying realizations Y_1, Y_2, and Y_3.

The GC method is incorporated into the proposed optimization procedure by adjusting the deformation parameter r in order to reduce mismatch between observed and simulated seismic data. For each combination of models, that is, for each value of r, we thus obtain a new set of V_p, V_s, ρ, and ϕ fields, for which the full-waveform synthetic seismic response d_{synth} is evaluated and compared to the observed seismic data d_{obs}. For this purpose, we use an elastic finite-difference time-domain approach [4] and consider an objective function defined as the root mean square (rms) error between d_{obs} and d_{synth} (e.g. Grana et al. [26])

$$J(r) = \sqrt{\frac{1}{N}\sum_{i=1,N}\left(d_{synth}(r) - d_{obs}\right)^2}, \tag{4}$$

where N is the number of the samples per trace and i the sample index. Our choice of the so-called L_2-norm for the objective function (4) is primarily motivated by the fact that most related studies also use this norm (e.g., Grana et al. [26]). Indeed, the L_2-norm corresponds to the maximum likelihood estimate for normally distributed data and errors (e.g., Menke [46]). The latter is a reasonably assumption for synthetic seismic data that are backscattered from stochastic reservoir models. It is, however, important to note that there are a number of potentially viable metric alternatives, such as the local dissimilarity map (e.g., Tillier et al. [59]) or the structural similarity index (e.g., Wang et al. [61]). While the choice of the norm is unlikely to have a significant influence on the final results for the considered synthetic test case, it may indeed be become decisive for the inversion of observed data, where the distribution of the

data and their errors may not be Gaussian and/or contain important outliers. In this context, it is important to note that the proposed stochastic inversion approach is particularly amenable to a flexible choice and parameterization of the objective function.

The GC model for which r minimizes the mismatch between synthetic and observed seismic data is then combined with two other initial SGCS realizations. This procedure is repeated until all initial realizations have been combined together. For each set of initial realizations, we thus ultimately obtain a reservoir model consisting of V_p, V_s, ρ, and ϕ fields that minimize the mismatch between the synthetic and the observed seismic data. This is illustrated by steps 1c and 1d in Fig. 1.

2.3 Dynamic optimization

The optimized models inferred so far honor the static data at the well locations as well as their second-order statistics throughout the model space. In the following, we seek to make these models consistent with the dynamic data documenting the injection and propagation of CO_2. To this end, we use a history matching procedure in which each iteration consists of the following steps:

1. run a fluid flow simulation on a combination of three models (Eq. 3);
2. apply suitable rock physics transforms to generate models of the elastic properties accounting for the injection and propagation of CO_2;
3. compute the seismic response;
4. calculate the mismatch between simulated and observed seismic data;
5. perturb the weights of the models to reduce the mismatch using GC.

The above procedure is repeated until the mismatch between the observed and synthetic seismic is minimal. A conceptually similar history matching approach, which is also based on L_2-norm, minimizing differences of compressional impedances between the base seismic survey and subsequent monitoring surveys to characterize the CO_2 distribution in the Utsira formation of the Sleipner field has recently been proposed by Fornel and Estublier [21].

2.3.1 Flow simulation

Modeling the time-lapse seismic response to CO_2 injection requires adequate fluid flow simulations to predict the migration of the CO_2 plume within the reservoir. Classic approaches rely on three-dimensional numerical solutions, which are accurate and versatile but for many purposes also prohibitive in terms of their computational cost. In recent years, approaches employing semi-analytical methods have been developed [52, 53]. One promising technique for the fast and accurate modeling of CO_2 injection and migration is based on the so-called vertical equilibrium (VE) assumption. VE models have a long tradition for describing fluid flow in porous media. In hydrology, this approach is known as the Dupuit approximation for unconfined aquifers (e.g., Møll Nilsen et al. [47]). In the oil and gas industry, corresponding models have been traditionally used to simulate multi-phase segregated flow (e.g., Martin [43]; Coats et al. [15]; Martin [44]). In recent years, VE methods have been employed to simulate large-scale CO_2 injection and migration in deep saline aquifers, where the inherent assumption of a sharp interface in conjunction with vertical equilibrium may be reasonable due to the large density difference between supercritical CO_2 and brine [13, 51, 52]. For the purpose of this work, we use the VE solver included in the Matlab Reservoir Simulation Toolbox (MRST) [40, 49] to simulate the injection and migration of CO_2 in a deep saline aquifer. We consider a two-phase model for the pore fluid (brine and CO_2), in which the distribution of the CO_2 plume is simply governed by the heterogeneity of the hydraulic properties.

2.3.2 Elastic properties

Elastic reservoir properties are usually computed through rock physics models, which transform previously inferred properties such as porosity, saturation, and mineralogy into P- and S-wave velocities and density. Here, we first estimate the elastic properties of the solid phase, that is, the bulk and shear moduli K_s and G_s, based on the arithmetic average of the upper and lower Hashin-Shtrikman bounds [31]. Then, we compute the elastic properties of the fluid phase, that is, the bulk modulus K_f and the density ρ_f, using mixing laws [6, 62]. The bulk modulus of the saturated rock K_{sat} is then estimated using Gassmann's relation [22] providing an estimate of the relaxed velocity at zero frequency, which is a lower bound of the fluid-saturation effect (e.g. Han and Batzle [29]). Inspite of significant inherent uncertainties, Gassmann's relation is widely used to predict and assess pore-fluid effects on sonic log and seismic velocity data (e.g. Njiekak et al. [50])

$$K_{sat} = K_{dry} + \frac{\left(1 - \frac{K_{dry}}{K_s}\right)^2}{\frac{\phi}{K_{fl}} + \frac{(1-\phi)}{K_s} - \frac{K_{dry}}{K_s^2}}. \tag{5}$$

The bulk and the shear moduli of the dry frame K_{dry} and G_{dry} are obtained from ultrasonic measurements on dry samples of the considered reservoir rocks [54]. The shear modulus of the saturated rock is assumed to correspond to its dry equivalent G_{sat}=G_{dry} [3]. The density ρ_{sat} is computed as a linear combination of the solid density ρ_s and

the fluid density ρ_f weighted by their respective volume fractions

$$\rho_{sat} = \phi\, \rho_f + (1-\phi)\rho_s. \tag{6}$$

The P- and S-wave velocities of the saturated rock are then given by

$$V_p = \sqrt{\left(\frac{K_{sat} + \frac{4}{3}G_{sat}}{\rho_{sat}}\right)}, \tag{7}$$

and

$$V_s = \sqrt{\frac{G_{sat}}{\rho_{sat}}}. \tag{8}$$

The full-waveform seismic response d_{synth} of this elastic model is computed using an elastic finite-difference time-domain approach [4] and the mismatch with regard to the corresponding observed data d_{obs} is evaluated using Eq. 4. The optimization procedure is basically the same as that used for the static reservoir data in step 1. At the end of the stochastic inversion process, we therefore obtain the spatial distributions of V_p, V_s, ρ, and ϕ that best honor the static and dynamic data, as schematically illustrated by step 2 in Fig. 1.

3 Application to a synthetic example based on a potential CO_2 injection site

In the following, we apply the workflow outlined above to a realistic synthetic test case based on a potential CCS pilot site in Southern Quebec, Canada. The Cambrian-Ordovician

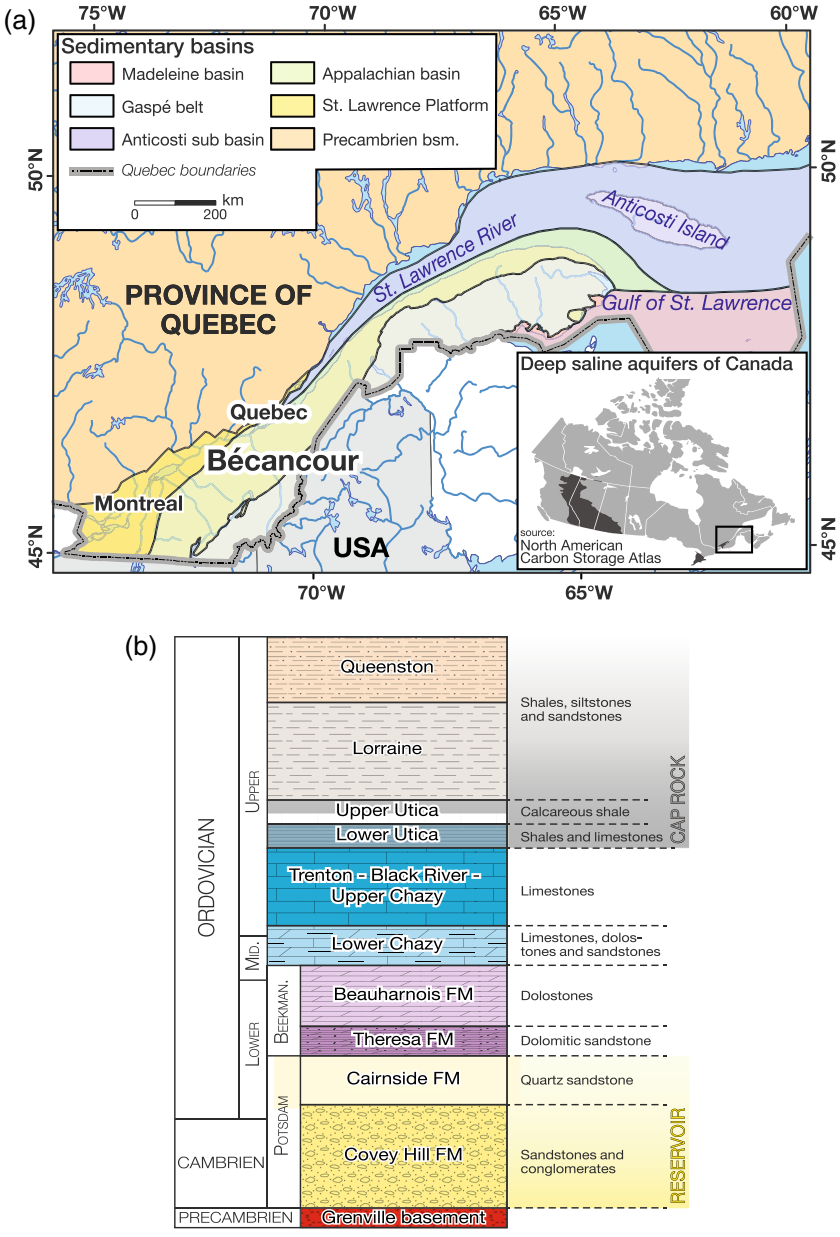

Fig. 2 **a** Geological setting and **b** stratigraphic sequence of the St. Lawrence Platform. Modified from Malo and Bédard [42] and Claprood et al. [14]

sedimentary basin of the St. Lawrence Platform (Fig. 2a) has been identified as the most prospective basin for CO_2 storage in the province of Quebec [42].

The prevailing stratigraphic sequence is shown in Fig. 2b. The Potsdam Group at the base of the sedimentary column lies unconformably upon the metamorphic Precambrian Grenville basement. It is comprised of the Cambrian sandstones and conglomerates of the Covey Hill formation (the target reservoir) and the lower Ordovician quartz sandstones of the Cairnside formation. The remainder of the sedimentary column is all of Ordovician age. The Beekmantown Group includes the dolomitic sandstones of the Theresa formation and the dolostones of the Beauharnois formation. The lower Chazy unit is composed of limestones, dolostones, and sandstones. The Trenton, Black River, and upper Chazy groups comprise essentially limestones. The Trenton Group is overlain by the Utica Shale and several hundred meters of interbedded shales, siltstones, and sandstones of the Lorraine Group. The lower Utica Shale comprises limestone beds and is more calcareous than the upper Utica Shale. Deep saline aquifers are found in the Trenton, Beekmantown, and Potsdam groups. Figure 3 shows synthetic well logs of V_p, ρ, and ϕ for the complete sedimentary sequence of the St. Lawrence Platform (Fig. 2b), which were compiled from a wide variety of log data available throughout the basin. *S*-wave velocities are computed using the Greenberg-Castagna relation [27] that is a simple average of the arithmetic and harmonic means of the compressional velocities of the mineralogical constituents. The sedimentary sequence is divided into seven units: Lorraine, Utica, Trenton, Beekmantown, Cairnside, Covey Hill, and Basement. For each unit, we estimated the mean values and the standard deviations of V_p, V_s, ρ, and ϕ based on the available log data throughout the basin (Table 1). Together with the corresponding cross-covariance characteristics of the logs, these statistical properties are used to generate both the synthetic well logs (Fig. 3) and the stochastic reference model of V_p, V_s, ρ, and ϕ through SGCS with the objective of respecting the observed transitions between the units (Fig. 4). It is important to note that the distribution of each

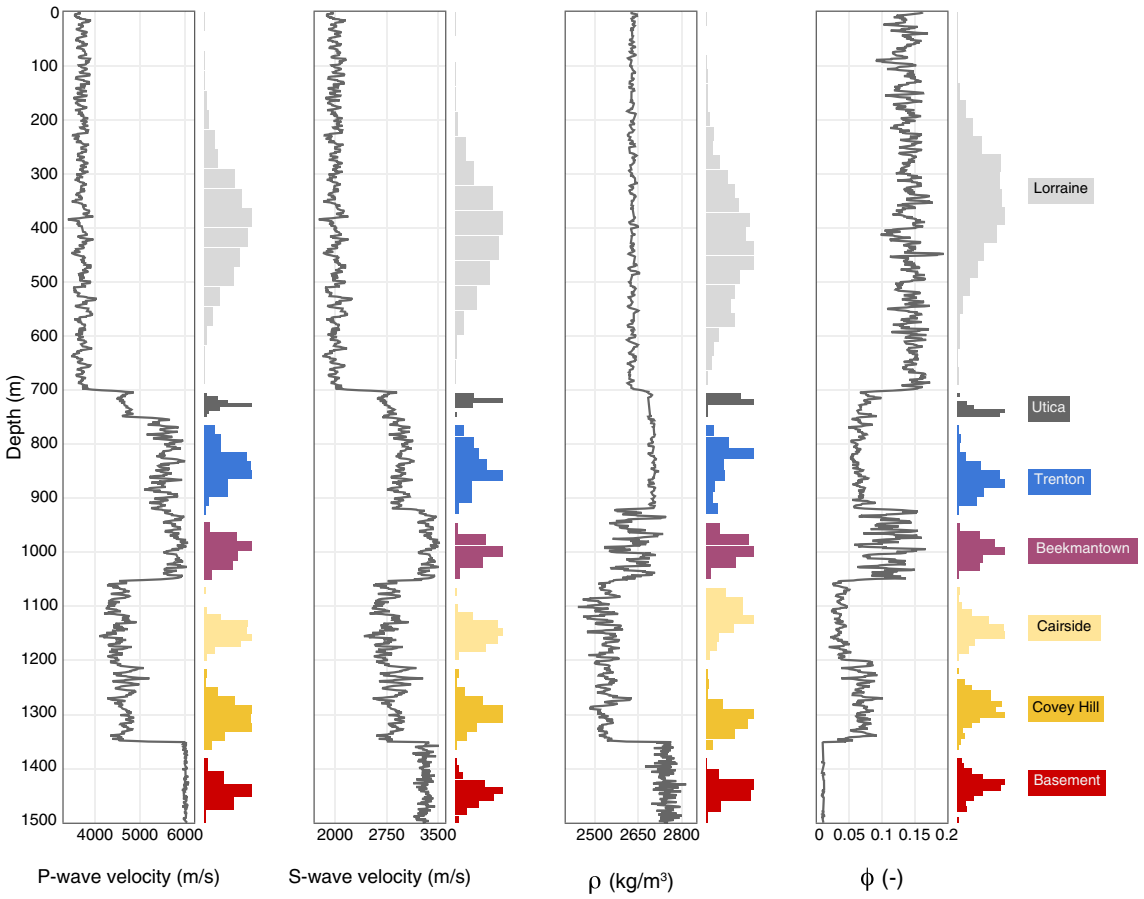

Fig. 3 Synthetic well logs of V_p, V_s, ρ, and ϕ that are considered to be representative of the sedimentary sequence of the St. Lawrence Platform. Also shown along the vertical axis are the histograms for these properties in the various sedimentary units, which together with the mean values and standard deviations shown in Fig. 1, clearly point to the quasi-Gaussian distribution of the considered parameters within the individual units as well as to the multi-modal nature of the corresponding global distributions

Table 1 Mean values and standard deviations of V_p, V_s, ρ, and ϕ within the various sedimentary units as inferred from a variety of well log data throughout the St. Lawrence Platform

Unit	Rock physical properties			
	V_p (m/s)	V_s (m/s)	ρ (kg/m^3)	ϕ (–)
Lorraine	3714 (98)	2003 (75)	2629 (7)	0.14 (0.01)
Utica	4671 (21)	2750 (8)	2688 (5)	0.07 (0.01)
Trenton	5538 (191)	2958 (83)	2700 (10)	0.06 (0.01)
Beekmantown	5766 (147)	3348 (85)	2635 (49)	0.11 (0.02)
Cairnside	4503 (172)	2739 (135)	2537 (49)	0.11 (0.01)
Covey Hill	4664 (171)	2849 (130)	2539 (26)	0.07 (0.01)
Basement	6002 (30)	3302 (72)	2746 (24)	0.01 (0.01)

property within each unit is approximately Gaussian, which is largely consistent with the corresponding evidence from the available well logs. Each parameter within a given formation is therefore adequately characterized by its mean and covariance. In the case of strongly non-Gaussian distributions, a normal score transform would have to be performed on each variable before the co-simulation.

The SGCS algorithm is built such that, for each pixel to simulate, it takes only the Gaussian distribution of the geological formation associated with the cell. Please note that

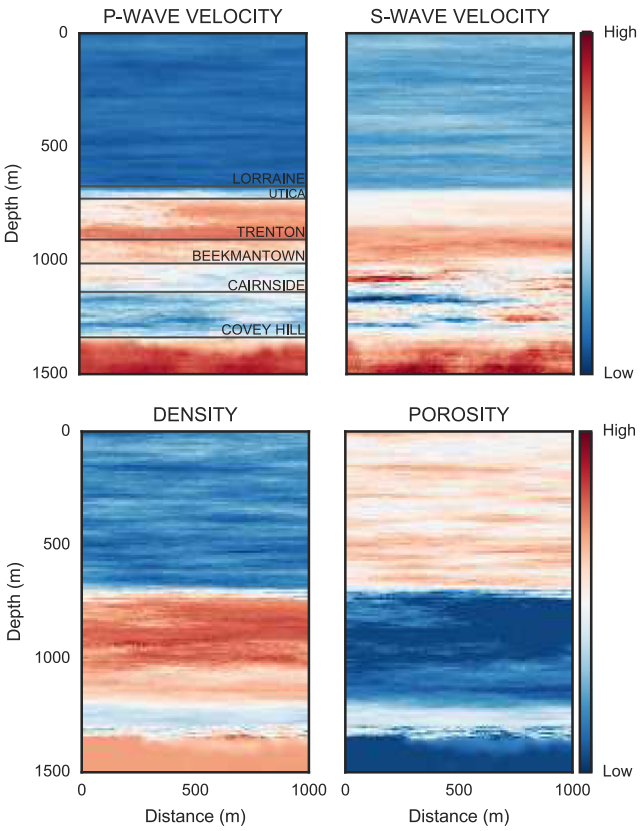

Fig. 4 Reference model for V_p, V_s, ρ, and ϕ

the functional characteristic of the covariance as well as the vertical correlation length are inferred from the available log data, whereas the horizontal correlation length is based on the conceptual model of the St. Lawrence Platform by Claprood et al. [14]. The dimension of the reference model is 1000 × 1500 m with a cell size of 1 × 1 m. The procedure followed for evaluating the seismic response of this reference model is based on Carcione et al. [11] who present an application of poro-viscoelastic modeling for monitoring CO_2 storage. This approach arguably represents the most accurate and rigorous way of accounting for the effects of the saturating pore fluids in the observed seismic data, because the effects of wave-induced fluid flow are naturally comprised in the governing equations. A full-waveform VSP for near, intermediate, and far offsets is modeled using the poro-viscoelastic algorithm of Giroux [23]. The elastic coefficients characterizing the porous media introduced by Biot and Willis [3] and reported in Carcione [10] are the P-wave modulus of the matrix

$$E = K_{dry} + \frac{4}{3}G, \tag{9}$$

the coupling modulus between the solid and the fluid

$$M = \frac{K_s^2}{D - K_{dry}}, \tag{10}$$

where the diffusion function D is defined as

$$D = K_s\left[1 + \phi(K_s K_f^{-1} - 1)\right], \tag{11}$$

and the poroelastic coefficient of effective stress

$$\alpha = 1 - \frac{K_{dry}}{K_s}. \tag{12}$$

K_{dry}, K_s, and K_f denote the bulk moduli of the drained matrix, the solid, and the fluid respectively; ϕ is porosity, and G the shear modulus of the matrix. Carcione [10] presented an approach to introduce viscoelasticity into Biot's poroelastic equations in which matrix-fluid mechanisms are

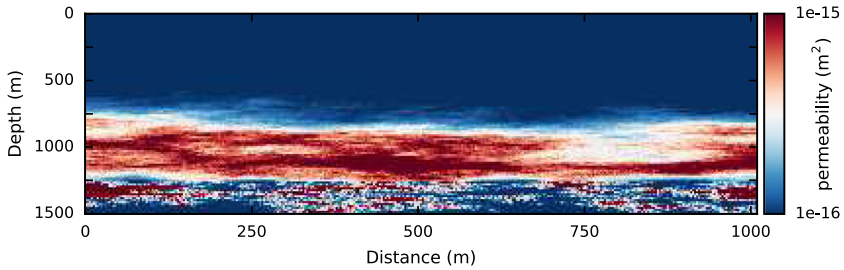

Fig. 5 Spatial distribution of permeability in the reservoir

modeled by generalizing the coupling modulus M to a time-dependent relaxation function, while the other elastic coefficients are independent of frequency. Detailed information on the implementation of the governing equations of motion can be found in Carcione [10] and Carcione and Helle [9].

As the ultimate aim of our inversion workflow is to obtain an elastic model of the reservoir which is consistent with the migration of the injected CO_2 over time. Considering a comprehensive range of offsets is essential to account for amplitude-versus-offset variations in the seismic response due changes in the saturating pore fluids. Based on the well logs and the complementary a priori information, we co-simulated five sets of 100 realizations each using SGCS. The choice of 100 realization per set is based on the fact that as the variance of all the realizations then reaches a plateau. These realizations of V_p, V_s, ϕ, and ρ are then linearly combined through GC to find the linear weights of the models that minimize the mismatch between the observed poro-viscoelastic seismic data generated for the reference model and synthetic seismic traces obtained for the optimzed model. At each step, synthetic full-waveform VSP data for near, intermediate, and far offsets are computed using an elastic finite-difference time-domain approach [4]. At the end of this iterative process, we obtain the global minima of the objective function (4), which is associated with the best static models for V_p, V_s, ρ, and ϕ.

As the time-lapse differences in the seismic response related to the injection and migration of CO_2 can be relatively weak and/or spatially localized, it is important to perform full-waveform forward modeling to capture the key aspects of the underlying physics in the synthetic seismic data. However, this step tends to be computationally very demanding. In this work, we therefore used a graphical processing unit (GPU) accelerated version of the viscoelastic finite-difference time-domain forward modeling algorithm

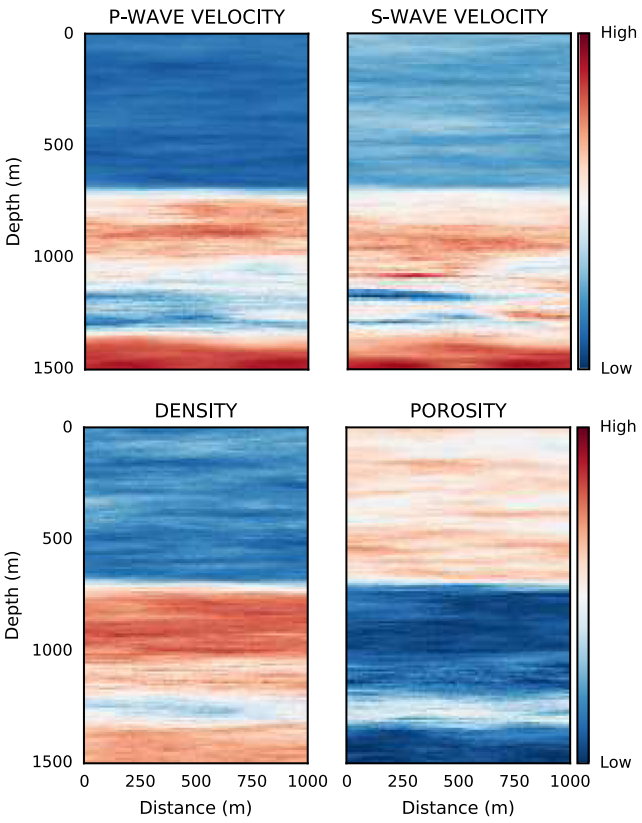

Fig. 6 Spatial distributions of V_p, V_s, ρ, and ϕ as inferred from the proposed two-step stochastic inversion procedure

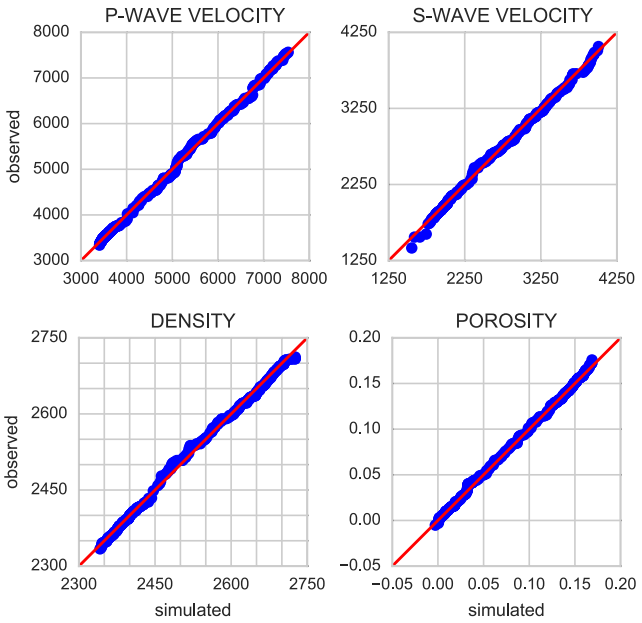

Fig. 7 Q-Q plots of observed versus simulated data for V_p, V_s, ρ, and ϕ

[4] developed by Fabien-Ouellet et al. [20]. This allows for reducing the run-time by more than two orders-of-magnitude compared to the original parallel version running on a 4-core CPU. The five realizations that best match the observed seismic data are again combined and optimized via GC parametrization with a CO_2 flow simulation being run at each iteration.

CO_2 is injected during 200 days into the Covey Hill formation, which consists of a low-porosity sandstone with a mean grain diameter of 5×10^{-6} m. The permeability

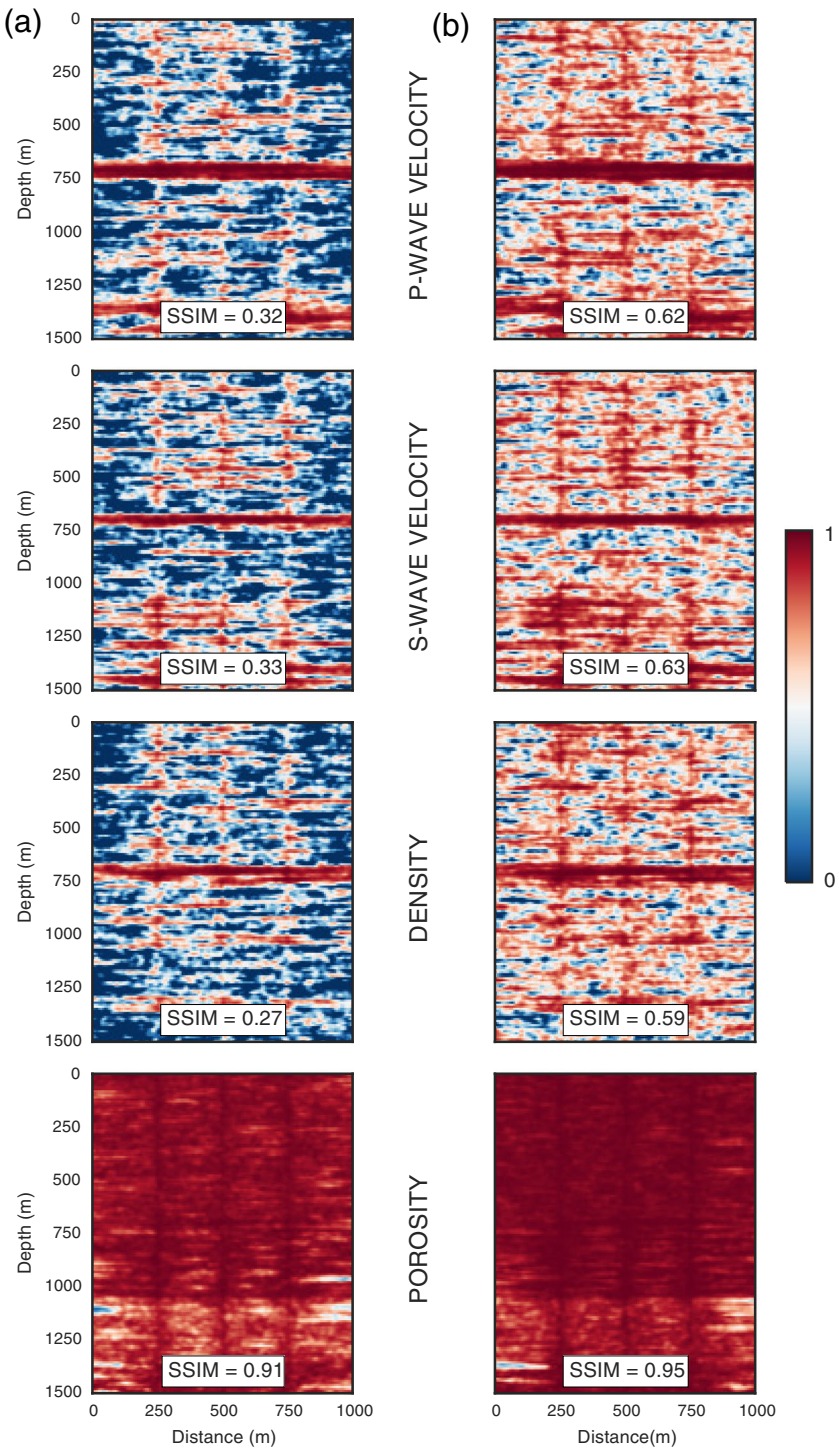

Fig. 8 Structural similarity index SSIM **a** between the reference model and one random SGCS realization and **b** between the reference model and the results of the proposed two-step stochastic inversion procedure

distribution for the reservoir sandstones is based on the Kozeny-Carman equation [12, 35, 45]

$$k = \frac{1}{72}\frac{\phi^3}{(1-\phi)^2\tau^2}d^2, \tag{13}$$

where d denotes the grain diameter and τ denotes tortuosity. The tortuosity is estimated following the approach proposed in Glover [24]. Figure 5 shows the spatial distribution of permeability within the reservoir for one of the five realizations. At each iteration, the elastic properties of the model in response to increasing CO_2 saturation are evaluated using Eqs. 10 to 14, and the mismatch of the corresponding synthetic seismic response with regard to the observed data is assessed. The final step of the inversion workflow provides distributions of V_p, V_s, ρ, and ϕ that best honor the static data as well as the effects of the injection and migration of CO_2 within the reservoir (Fig. 6). In this context, it is important to note that the considered reservoir model corresponds to a particularly challenging scenario due to its low porosity and permeability.

3.1 Model assessment and validation

A key objective of stochastic simulations is to obtain a result that honors the probability density function of the observed data. The quantile-quantile or Q-Q plot is best suited to assess the similarity between two distributions. Figure 7 shows the Q-Q plot for the reference model and the inversion results. Almost all points lie on the 45°-reference line, which confirms that, despite the multi-modal nature of the global distribution evidenced in Fig. 3, the probability density function of the inversion results honors the one of the reference model.

Another key metric is the structural similarity index (SSIM), which compares local patterns between two images and is based on the computation of three terms: the luminance term l, the contrast term c, and the structural term s. The overall index is a multiplicative combination of the three terms [61]

$$SSIM(x,y) = \left[l(x,y)\right]^{\alpha}\left[c(x,y)\right]^{\beta}\left[s(x,y)\right]^{\gamma} \tag{14}$$

with

$$\begin{aligned} l(x,y) &= \frac{2\mu_x\mu_y + C_1}{\mu_x^2 + \mu_y^2 + C_1}, \\ c(x,y) &= \frac{2\sigma_x\sigma_y + C_2}{\sigma_x^2 + \sigma_y^2 + C_2}, \\ s(x,y) &= \frac{\sigma_{xy} + C_3}{\sigma_x + \sigma_y + C_3}, \end{aligned} \tag{15}$$

where μ_x, μ_y, σ_x, σ_y, and σ_{xy} are the local means, standard deviations, and the cross-covariance of the images x and y, and $C1$, $C2$, and $C3$ are constants. The exponents α, β, and γ are parameters used to adjust the relative importance of the three components. SSIM assumes values between 0 and 1, where the limiting case of a SSIM of 1 corresponds to two identical data sets. Figure 8 shows the SSIM between the reference model and one random SGCS and between the reference model and the inversion result for P- and S-wave velocities, density, and porosity. The inversion result has a SSIM of approximately 0.6 for V_p, V_s, and ρ, which is significantly higher than the SGCS realization. Conversely, ϕ shows a SSIM index close to 1 for both the SGCS realization and the inversion results, which is primarily due to its low variance (Table 1). In this context, it is important to note that we observe the clearest improvement of the similarity for the inversion results (SSIM = 0.89) compared that of the SGCS (SSIM = 0.82) at the reservoir level, that is, at

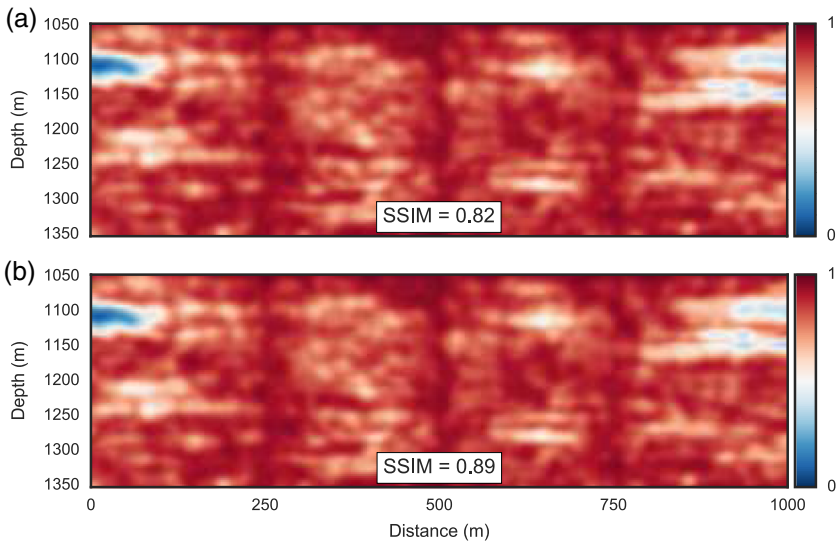

Fig. 9 Structural similarity index SSIM **a** between the reference model of the porosity and one random SGCS realization and **b** between the reference model of the porosity and the corresponding inversion result

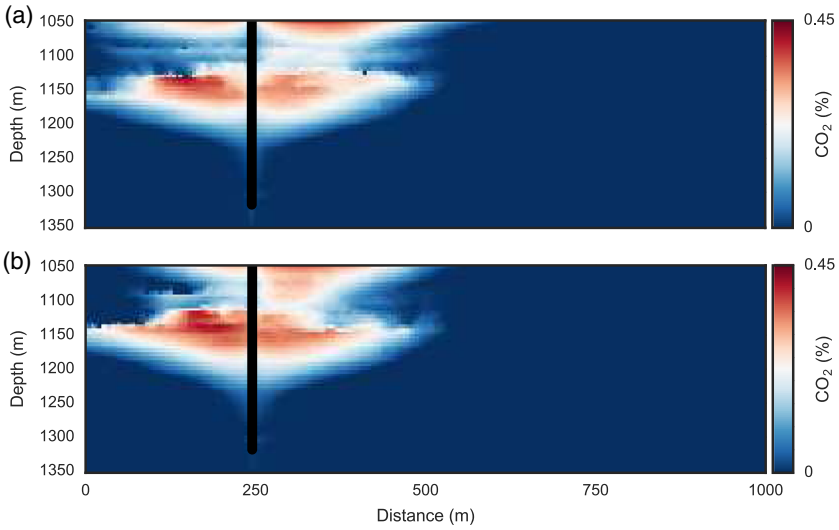

Fig. 10 CO_2 distribution after 300 days of injection for **a** the reference model and **b** the inverted model. The vertical black lines denotes the injection well

depths of 1050 to 1300 m (Fig. 9). This is the direct consequence of the additional information and constraints added by the dynamic data, which in turn illustrates the suitability of the proposed two-step stochastic inversion approach for the considered task. Figure 10 shows the spatial distribution of CO_2 after 300 days from the start of the injection for both the reference model (Fig. 10a) and the inverted model (Fig. 10b). The similarity between the two images is confirmed by a SSIM of 0.94.

4 Conclusion

The objective of this study was to develop an inversion workflow to infer reservoir properties such as V_p, V_s, ρ, and ϕ that are sufficiently detailed and accurate to allow for reliable monitoring of the spatial distribution of CO_2. To this end, we developed a two-step optimization procedure based on GC for both static and dynamic reservoir characterization. The choice of a two-step approach is motivated by three factors: (1) the optimization of the static parameters before injection permits to decrease the number of models before the injection. Consequently, it allows to reduce the number of computationally expensive CO_2 transport simulations; (2) in actual CO_2 injection projects, the required data are always available before injection; (3) SGCS are maximizing the entropy, which implies that the range of the variance is maximal between different models as well as within a given model. Optimizing for the static parameters before injection reduces the starting ensemble to a set of models that have already been calibrated to seismic data and hence show a smaller uncertainty than the starting ensemble. It is then more probable that the global spatial heterogeneity of the parameters is close to the true one. The use of dynamic data will then mostly refine the distribution of the extreme values of the hydraulic parameters.

Numerical experiments based on a realistic model of a heterogeneous saline aquifer indicate that the methodology allows for accurately inferring the spatial distribution of the static reservoir properties. The method then uses this static model to simulate the injection and migration of CO_2 as well as its effects on the seismic response. Applying the proposed inversion approach to time-lapse VSP data permits to reliably characterize the migration of the CO_2 plume. The proposed workflow is extremely versatile and not limited to seismic data, but can be applied to any kind of geophysical measurements that are sensitive to changes in CO_2 concentration. Future work will need to explore the application of this methodology to field data as well as its extension to three-dimensional scenarios.

Acknowledgments The authors would like to thank G. Fabien-Ouellet for providing the GPU-accelerated viscoelastic finite-difference time-domain code. We also acknowledge the reviewers for the helpful comments and suggestions. Financial support was provided by a research grant from the Quebec Ministry of Sustainable Development, Environment, Fauna and Parks and the Canada Research Chair in Assimilation of Geological and Geophysical Data for Stochastic Geological Modeling. Part of this work has been completed within the Swiss Competence Center for Energy Research - Supply of Electricty with support form the Swiss Commission for Technology and Innovation.

References

1. Avseth, P., Mukerji, T., Jørstad, A., Mavko, G., Veggeland, T.: Seismic reservoir mapping from 3-D AVO in a North Sea turbidite system. Geophysics **66**, 1157–1176 (2001)
2. Azevedo, L., Nunes, R., Correia, P., Soares, A., Guerreiro, L., Neto, G.S.: Multidimensional scaling for the evaluation of a geostatistical seismic elastic inversion methodology. Geophysics **79**, M1–M10 (2013)
3. Biot, M.A., Willis, D.G.: The elastic coefficients of the theory of consolidation. J. Appl. Mech. **24**, 594–601 (1957)

4. Bohlen, T.: Parallel 3-D viscoelastic finite difference seismic modelling. Comput. Geosci. **28**, 887–899 (2002)
5. Bosch, M., Carvajal, C., Rodrigues, J., Torres, A., Aldana, M., Sierra, J.: Petrophysical seismic inversion conditioned to well-log data: methods and application to a gas reservoir. Geophysics **74**, O1–O15 (2009)
6. Brie, A., Pampuri, F., Marsala, A., Meazza, O.: Shear sonic interpretation in gas-bearing sands. SPE Annual Technical Conference and Exhibition (1995)
7. Buland, A., Omre, H.: Bayesian linearized AVO inversion. Geophysics **68**, 185–198 (2003)
8. Caers, J., Hoffman, T.: The probability perturbation method: a new look at Bayesian inverse modeling. Math. Geol. **38**, 81–100 (2006)
9. Carcione, J., Helle, H.: Numerical solution of the poroviscoelastic wave equation on a staggered mesh. J. Comput. Phys. **154**, 520–527 (1999)
10. Carcione, J.M.: Viscoelastic effective rheologies for modelling wave propagation in porous media. Geophys. Prospect. **46**, 249–270 (1998)
11. Carcione, J.M., Picotti, S., Gei, D., Rossi, G.: Physics and seismic modeling for monitoring CO_2 storage. Pure Appl. Geophys. **163**, 175–207 (2006)
12. Carman, P.: The determination of the specific surface of powders. J. Soc. Chem. Ind. **57**, 225–234 (1938)
13. Celia, M., Bachu, S., Nordbotten, J., Kavetski, D., Gasda, S.: A risk assessment tool to quantify CO_2 leakage potential through wells in mature sedimentary basins. In: Proceedings of the 8th Conference on Greenhouse Gas Technologies (2006)
14. Claprood, M., Gloaguen, E., Giroux, B., Konstantinovskaya, E., Malo, M., Duchesne, M.J.: Workflow using sparse vintage data for building a first geological and reservoir model for CO_2 geological storage in deep saline aquifer. A case study in the St. Lawrence Platform, Canada. Greenh. Gases Sci. Technol. **2**, 260–278 (2012)
15. Coats, K., Nielsen, R., Terhune, M.H., Weber, A.: Simulation of three-dimensional, two-phase flow in oil and gas reservoirs. Soc. Petroleum Eng. J. **7**, 377–388 (1967)
16. Deutsch, C.V., Journel, A.G.: GSLIB: Geostatistical Software Library and User's Guide (Applied Geostatistics). Oxford University Press (1997)
17. Doyen, P.: Seismic Reservoir Characterization: An Earth Modelling Perspective. EAGE (2007)
18. Eidsvik, J., Avseth, P., Omre, H., Mukerji, T., Mavko, G.: Stochastic reservoir characterization using prestack seismic data. Geophysics **69**, 978–993 (2004)
19. EU: Report from the commission to the European parliament and the council on the implementation of Directive 2009/31/EC on the geological storage of carbon dioxide. Technical Report. European Union (2014)
20. Fabien-Ouellet, G., Gloaguen, E., Giroux, B.: Viscoelastic forward and adjoint modeling with OpenCL on heterogeneous clusters. In: 78th EAGE Conference & Exhibition. Vienna (2016)
21. Fornel, A., Estublier, A.: To a dynamic update of the Sleipner CO_2 storage geological model using 4D seismic data. Energy Procedia **37**, 4902–4909 (2013)
22. Gassmann, F.: Elastic waves through a packing of spheres. Geophysics **16**, 673–685 (1951)
23. Giroux, B.: Performance of convolutional perfectly matched layers for pseudospectral time domain poroviscoelastic schemes. Comput. Geosci. **45**, 149–160 (2012)
24. Glover, P.: What is the cementation exponent? A new interpretation. Lead. Edge **28**, 82–85 (2009)
25. González, E.F., Mukerji, T., Mavko, G.: Seismic inversion combining rock physics and multiple-point geostatistics. Geophysics **73**, R11–R21 (2008)
26. Grana, D., Mukerji, T., Dvorkin, J., Mavko, G.: Stochastic inversion of facies from seismic data based on sequential simulations and probability perturbation method. Geophysics **77**, M53—M72 (2012)
27. Greenberg, M.L., Castagna, J.P.: Shear-wave velocity estimation in porous rocks: theoretical formulation, preliminary verification and applications. Geophys. Prospect **40**, 195–209 (1992)
28. Gunning, J., Glinsky, M.E.: Detection of reservoir quality using Bayesian seismic inversion. Geophysics **72**, R37–R49 (2007)
29. Han, D.h., Batzle, M.L.: Gassmann's equation and fluid-saturation effects on seismic velocities. Geophysics **69**, 398–405 (2004)
30. Hansen, T.M., Cordua, K.S., Mosegaard, K.: Inverse problems with non-trivial priors: efficient solution through sequential Gibbs sampling. Comput. Geosci. **16**, 593–611 (2012)
31. Hashin, Z., Shtrikman, S.: A variational approach to the theory of the elastic behaviour of multiphase materials. J. Mech. Phys. Solids **11**, 127–140 (1963)
32. Hu, L.Y.: Gradual deformation and iterative calibration of Gaussian-related stochastic models. Math. Geol. **32**, 87–108 (2000)
33. Hu, L.Y.: Combination of dependent realizations within the gradual deformation method. Math. Geol. **34**, 953–963 (2002)
34. Hu, L.Y., Blanc, G., Noetinger, B.: Gradual deformation and iterative calibration of sequential stochastic simulations. Math. Geol. **33**, 475–489 (2001)
35. Kozeny, J.: Über kapillare Leitung des Wassers im Boden. Akad. Wiss. Wien **136**, 271–306 (1927)
36. Larsen, A.L., Ulvmoen, M., Omre, H., Buland, A.: Bayesian lithology/fluid prediction and simulation on the basis of a Markov-chain prior model. Geophysics **71**, R69–R78 (2006)
37. Le Ravalec, M.: Inverse Stochastic Modeling of Flow in Porous Media: Applications to Reservoir Characterization. Editions OPHRYS (2005)
38. Le Ravalec, M., Mouche, E.: Calibrating transmissivities from piezometric heads with the gradual deformation method: an application to the Culebra Dolomite unit at the Waste Isolation Pilot Plant (WIPP), New Mexico, USA. J. Hydrol. **472-473**, 1–13 (2012)
39. Le Ravalec, M., Noetinger, B., Hu, L.Y.: The FFT moving average (FFT-MA) generator: an efficient numerical method for generating and conditioning Gaussian simulations. Math. Geol. **32**, 701–723 (2000)
40. Lie, K.A.: An Introduction to reservoir simulation using Matlab: User guide for the Matlab Reservoir Simulation Toolbox (MRST). Technical Report. SINTEF ICT. Oslo, Norway (2015)
41. Lumley, D., Sherlock, D., Daley, T., Huang, L., Lawton, D., Masters, R., Verliac, M., White, D.: Highlights of the 2009 SEG Summer Research Workshop on CO_2 Sequestration. Lead. Edge **29**, 138–145 (2010)
42. Malo, M., Bédard, K.: Basin-scale assessment for CO_2 storage prospectivity in the province of Québec, Canada. Energy Procedia **23**, 487–494 (2012)
43. Martin, J.C.: Some mathematical aspects of two phase flow with application to flooding and gravity segregation. Prod. Month. **22**(6), 22–35 (1958)
44. Martin, J.C.: Partial integration of equations of multiphase flow. Soc. Petroleum Eng. J. **8**, 370–380 (1968)
45. Mavko, G., Mukerji, T., Dvorkin, J.: The Rock Physics Handbook: Tools for Seismic Analysis of Porous Media. Cambridge University Press (2009)
46. Menke, W.: Geophysical data analysis: Discrete inverse theory, vol. 45. Academic Press (2012)

47. Møll Nilsen, H., Herrera, P.A., Ashraf, M., Ligaarden, I., Iding, M., Hermanrud, C., Lie, K.A., Nordbotten, J.M., Dahle, H.K., Keilegavlen, E.: Field-case simulation of CO_2-plume migration using vertical-equilibrium models. Energy Procedia **4**, 3801–3808 (2011)
48. Mukerji, T., Jørstad, A., Avseth, P., Mavko, G., Granli, J.R.: Mapping lithofacies and pore-fluid probabilities in a North Sea reservoir: seismic inversions and statistical rock physics. Geophysics **66**, 988–1001 (2001)
49. Nilsen, H.M., Lie, K.A., Andersen, O.: Fully-implicit simulation of vertical-equilibrium models with hysteresis and capillary fringe. Comput. Geosci. **20**, 49–67 (2016)
50. Njiekak, G., Schmitt, D.R., Yam, H., Kofman, R.S.: CO_2 rock physics as part of the Weyburn-Midale geological storage project. Int. J. Greenhouse Gas Control **16**, S118–S133 (2013)
51. Nordbotten, J., Celia, M.: Analysis of plume extent using analytical solutions for CO_2 storage. In: Proceedings of the 16th conference on Computational Methods in Water Resources (2006)
52. Nordbotten, J.M., Celia, M.A., Bachu, S.: Injection and storage of CO_2 in deep saline aquifers: analytical solution for CO_2 plume evolution during injection. Transport Porous Media **58**, 339–360 (2005)
53. Nordbotten, J.M., Kavetski, D., Celia, M.A., Bachu, S.: Model for CO_2 leakage including multiple geological layers and multiple leaky wells. Environ. Sci. Technol. **43**, 743–749 (2009)
54. Perozzi, L., Giroux, B., Kofman, R., Schmitt, D.: Preparatory work for the seismic monitoring of CO_2 storage at a prospective site in the St. Lawrence Lowlands, Canada. In: 76th European Association of Geoscientists and Engineers Conference and Exhibition - Amsterdam (2014)
55. Ramirez, A., White, D., Hao, Y., Dyer, K., Johnson, J.: Estimating reservoir permeabilities using the seismic response to CO_2 injection and stochastic inversion. Int. J. Greenhouse Gas Control **16**, S146–S159 (2013)
56. Rimstad, K., Omre, H.: Impact of rock-physics depth trends and Markov random fields on hierarchical Bayesian lithology/fluid prediction. Geophysics **75**, R93–R108 (2010)
57. Roggero, F., Hu, L.: Gradual deformation of continuous geostatistical models for history matching. SPE Annual Technical Conference and Exhibition (1998)
58. Tarantola, A.: Inverse Problem Theory and Methods for Model Parameter Estimation. SIAM: Society for Industrial and Applied Mathematics (2004)
59. Tillier, E., Le Ravalec, M., Da Veiga, S.: Simultaneous inversion of production data and seismic attributes: application to a synthetic SAGD produced field case. Oil Gas Sci. Technol. Rev. IFP Energies nouvelles **67**, 289–301 (2012)
60. Ulvmoen, M., Omre, H.: Improved resolution in Bayesian lithology/fluid inversion from prestack seismic data and well observations: Part 1 - Methodology. Geophysics **75**, R21–R35 (2010)
61. Wang, Z., Bovik, A., Sheikh, H., Simoncelli, E.: Image quality assessment: from error visibility to structural similarity. IEEE Trans. Image Process. **13**, 600–612 (2004)
62. Wood, A.: A Textbook of Sound: Being an Account of the Physics of Vibrations with Special Reference to Recent Theoretical and Technical Developments. G. Bell and Sons Limited (1955)
63. Ying, Z., Gomez-Hernandez, J.: An improved deformation algorithm for automatic history matching. Report 13, Stanford Center for Reservoir Forecasting (SCRF) Annual Report. Stanford (2000)